This preprint is accepted for publication as the following book chapter:

Sajjadinia, Seyed Shayan, Bruno Carpentieri, and Gerhard A. Holzapfel. "Hybrid Data-Driven and Numerical Modeling of Articular Cartilage." In Carpentieri, Bruno and Lecca, Paola (Eds.), Big Data Analysis and Artificial Intelligence for Medical Sciences (2024): 181-203.

Hybrid Data-Driven and Numerical Modeling of Articular Cartilage

Seyed Shayan Sajjadinia,[1*] Bruno Carpentieri,[1] and Gerhard A. Holzapfel[2,3]

[1] *Faculty of Engineering, Free University of Bozen-Bolzano, 39100, Bozen-Bolzano, Italy*
[2] *Institute of Biomechanics, Graz University of Technology, 8010, Graz, Austria*
[3] *Department of Structural Engineering, Norwegian University of Science and Technology, Trondheim, Norway*

*Corresponding Author: Seyed Shayan Sajjadinia; ssajjadinia@unibz.it

Abstract: While numerical models provide indispensable tools for solving advanced physics problems, reducing their high computational costs is a highly active research topic. Artificial intelligence (AI) is often used for this purpose by defining data-driven and high-performance models that learn to mimic the numerical models and eventually replace them with machine learning (ML). In this study, we review these so-called surrogate models, but with a focus on advanced articular cartilage (AC) modeling. AC is a low-friction soft tissue with excellent load-bearing capacities that covers and protects articulating bones, but given the high prevalence of cartilage damage due to biomechanical factors, surrogate models are used to efficiently study the multi-physics, particularly the biomechanics, of AC. To that end, we familiarize the readers with the key biological, numerical, and learning aspects of AC models. In particular, the implicit FE modeling as a well-founded numerical method is

briefly explained in order to clarify its benefits and complexity at the same time. Next, we give a detailed overview of the relevant ML algorithms, and it is shown that while the general-purpose ML models can be used as a surrogate for the AC FE simulation, they potentially require large and expensive numerical datasets. This can be handled by hybrid surrogates, which are based on the application of simplified numerical models in the ML surrogates. We conclude this chapter by discussing future directions.

Keywords: biomechanics, articular cartilage, artificial intelligence, finite element method, machine learning

1.1. Introduction

Articular cartilage (AC) is a load-bearing and lubricating soft tissue between articulating bony ends, which under healthy conditions exhibits excellent resistance and shock-absorbing abilities [Lu and Mow, 2008]. Nevertheless, the damage to this tissue, especially due to biomechanical factors, causes significant health care costs [Salmon et al., 2016]. Therefore, the analyses of cartilage is a very active area in the biomedical sciences, hopefully to prevent or detect damage in its early stages, which requires a good understanding of the biomechanics involved [Martínez-Moreno et al., 2019].

Artificial intelligence (AI), particularly using machine learning (ML), has made significant strides in biomechanical cartilage studies. These advancements are evident in recent investigations on the heterogeneous material characterization of knee cartilage [Hamsayeh Abbasi Niasar and Li, 2023], damage classification through unique biomechanical markers [Alunni Cardinali et al., 2023], and fiber orientation prediction in tissue [Mirmojarabian et al., 2023]. However, the acquisition of clinical data for training these models is

still a considerable challenge. This limitation has led to a predominant preference for physics-based models, especially using numerical methods.

Numerical modeling, notably using finite element (FE) methods, is crucial in solving (and approximating) cartilage-related physics problems [Freutel et al., 2014]. Such methods find application in many scenarios: simulating crack propagation under cyclic loading [Orozco et al., 2022], analyzing fibrillar components [Sajjadinia and Haghpanahi, 2021], and comparing healthy and damaged tissues [Vulović et al., 2021], to name a few. Despite their functionality, these techniques are highly iterative algorithms with significant computation time, varying from minutes to days based on the hardware settings and simulation definitions [Haut Donahue et al., 2002, Kazemi et al., 2011, Naghibi Beidokhti et al., 2016, Wang and Yang, 2018, Lostado Lorza et al., 2021].

One method to overcome the high computational costs of numerical simulations, including cartilage analyses, is to use ML to create similar data-driven models. These models that learn the behavior of numerical models by samples extracted from them are usually far faster than the main numerical models that can be used instead of them; hence, they are called surrogates. Surrogates of biomechanical cartilage models receive special attention, see, e.g., Paiva et al. [2012], Arbabi et al. [2016a,b], Egli et al. [2021], Sajjadinia et al. [2022]. One goal of this chapter is to revisit these models and relevant issues, with a focus on hybrid paradigms that use both physics-based and data-driven approaches.

This study is organized as follows: Section 1.2 first summarizes the role of cartilage in joint biomechanics and next the cartilage components in load-

bearing. Section 1.3 first gives a general picture of numerical modeling, followed by a brief explanation of an example of advanced constitutive (material) equations to get a better understanding of their application and complexity. Section 1.4 gives an overview of the most important methods of ML with regular and hybrid algorithms, while Section 1.5 concludes this work.

1.2. Knee and Cartilage

1.2.1. Main joint substructures

A tibiofemoral joint is the largest joint within the knee and entire body (as shown in Figure 1.1), consisting of the touching long ends of bones (namely femur and tibia), cartilaginous tissue (including femoral cartilage, tibial cartilage, and menisci) and ligaments. The shape of the bones allows condyloid joints, while the cam shape of the femoral condyles allows rotation in all axes [Goldblatt and Richmond, 2003]. The asymmetry within this joint was created over the course of evolution to accommodate the joint to the complex asymmetrical dynamics of the knee caused by various musculoskeletal movements of the body, e.g., with the regular gait [Dye, 1987].

Soft tissues play a key role in protecting the knee capsule from pathological motion and conditions. Ligaments stabilize it and avoid unphysiological positions and movements. Meniscus substructures, with their wedge-like cross-sections, allow the distribution of the axial force on articulating surfaces; this reduces the peak contact pressure [Walker and Erkman, 1975, Mameri et al., 2022]. In addition, AC absorbs this compressive distributed force and

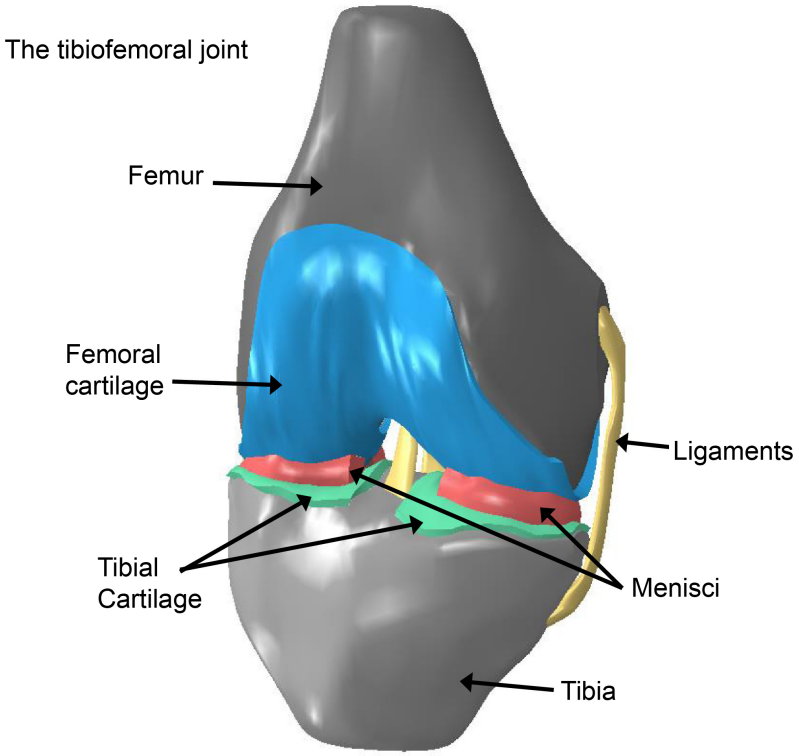

Figure 1.1: Main substructures in a knee model: Image is extracted from Cooper et al. [2019] under its CC BY 4.0 license, permitting reuse with a proper citation.

enables a low-friction sliding motion [Forster and Fisher, 1996]. Although meniscal tissue has a cartilage-like composition with different but similar biomechanical roles [Danso et al., 2014, Chen et al., 2017], we particularly focus on AC due to its high importance in osteoarthritis studies [Buckwalter, 1995, Pearle et al., 2005, Goldring, 2012, Brody, 2015].

Osteoarthritis, a degenerative joint disease, predominantly impairs cartilage by gradually deteriorating its structure, leading to joint pain, discomfort, and eventual loss of joint function [Lespasio et al., 2017]. It affects roughly a third of individuals aged 65 and above, with a notable predominance in

women, thereby incurring significant socioeconomic costs on healthcare systems [Chen et al., 2012, Hawker, 2019]. Despite an incomplete understanding of the precise mechanism, recent review studies highlight potential correlations, including lifestyle elements such as poor diet, some comorbidities like diabetes, biomechanical factors (e.g., traumatic injuries), and hereditary aspects such as genetic risk loci [Loeser et al., 2016, Mobasheri et al., 2017, Astephen Wilson and Kobsar, 2021].

In light of these correlations, biomechanical studies have proven essential in shaping strategies for rehabilitation and exercise [Kong et al., 2022]. On the other hand, AC, much like other connective tissues, gains its functional properties largely from extracellular components, specifically collagen fibrils and proteoglycan proteins [Culav et al., 1999, Brody, 2015]. Consequently, a large focus of biomechanical research involves simulating the interaction of these components or phases [Klika et al., 2016, Ebrahimi et al., 2019, Sajjadinia et al., 2019, Lin et al., 2021, Paz et al., 2022], which is outlined in the following subsection.

1.2.2. Load-bearing cartilage phases

Aggrecans, the most common proteoglycan molecules in AC, are connected to the chains of hyaluronic acid to form large aggregates that are trapped in the collagen network. Because of their constituent glycosaminoglycan (GAG), which are negatively charged compounds, they have a fixed negative charge, resulting in a chemical potential gradient that attracts water to achieve chem-

ical equilibrium, i.e. the mechanism of osmosis [Kiani et al., 2002, Gómez-Florit et al., 2020, Johnson et al., 2021]. The aggregates are then responsible for the vital osmotic pressure that contributes to the load-bearing of the tissue by counteracting the applied loads. Moreover, this internal pressure swells the tissue, which is compensated by stretching of the collagen network, which increases the reversible deformation of the tissue [Dudhia, 2005].

Thanks to the osmotic pressure of AC and the porous structure of the tissue, water makes up about 60–80% of the tissue [Cederlund and Aspden, 2022]. This not only maintains perfect lubrication on the surface of AC but also resists external loads as the hydrostatic fluid pressure, usually more than the other load-bearing components [Quiroga et al., 2017, Sajjadinia et al., 2019]. Together with the solid constituents, the tissue can then be viewed as a biphasic mixture with a fluid phase and an effective solid phase (considering the overall effect of solid components such as aggregates and collagen networks). In addition, the water flow in the small solid pores at the beginning of cartilage deformation creates a considerable drag force between the two phases, which balance out over time [Mow et al., 1980]. This results in a greater resistance to tissue deformation, which is regularly determined by the level of permeability [Eschweiler et al., 2021].

Besides, collagen fibrillar networks reinforce AC against tensile forces, like structural wire ropes [Bozec et al., 2007, Bielajew et al., 2020]. It is observed that the fibrils can be classified into primary anisotropic (direction-dependent) and secondary isotropic (direction-independent) bundles [Clark, 1985, Wilson et al., 2004]. The isotropic bundles of the healthy tissue tend to

be oriented roughly parallel to and between all axes of Euclidean (geometrical) space, while the anisotropic bundles are oriented in an arcade-like fashion: they extend perpendicularly from the calcified regions in the deep zone of AC and gradually rotate in the middle zone to become parallel to the AC surface [Wilson et al., 2004]. While the fibrils are anchored to the bones in this way, they protect the surface from shear-induced damages [Shirazi and Shirazi-Adl, 2008, Motavalli et al., 2014].

For further clarification, Figure 1.2 is extracted from an osteoarthritis study, which represents one of the possible scenarios in this condition, assuming that AC is viscoelastic: while elasticity describes the reversible deformation of the tissue, viscosity is the energy loss during this deformation (e.g., due to drag force). In this particular case, the main measurable material properties, including the storage and loss moduli, correspond to the ability to store elastic energy and the ability to dissipate energy, respectively [Banks et al., 2011]. However, in a more general formulation of AC biomechanics, calculating the precise long-term and short-term local responses requires multi-physics constitutive equations (which simultaneously account for at least some of the above-mentioned constituents). Because of their complexity, they are implemented by some numerical approximation methods, e.g., the FE method [Freutel et al., 2014].

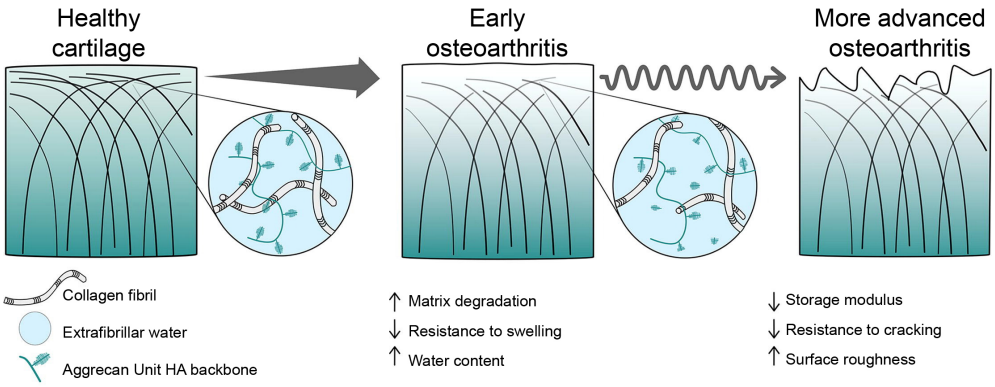

Figure 1.2: A possible scenario for osteoarthritis in articular cartilage is as follows: in the early stages, the tissue matrix undergoes degradation, resulting in an increase in water content. However, in more advanced conditions, it manifests itself through wear and tear on the tissue surface. The image has been modified from Cooke et al. [2018] under its CC BY 4.0 license, allowing for reuse with correct citation. Abbreviation: HA = hyaluronic acid.

1.3. Physics-based modeling

1.3.1. Numerical modeling

In cartilage modeling, the effects of weight and inertia are usually ignored, given the low density of the tissue [Pearle et al., 2005]. By applying Newton's second law, we can argue that any force exerted on the tissue boundary, i.e., surface traction, should be balanced (although it can deform the model to reach equilibrium). This balance can be illustrated by the following simplified equilibrium equation in 3D Euclidean space, i.e.

$$\int_s \mathbf{t} \mathrm{d}S = \mathbf{0}, \tag{1.1}$$

where S is the surface area of the deformed solid material, and $\mathbf{t}$ is the surface traction, which is correlated with the total Cauchy stress tensor $\boldsymbol{\sigma}_{\mathrm{T}}$ as

$$\mathbf{t} = \boldsymbol{\sigma}_{\mathrm{T}} \cdot \mathbf{n}, \tag{1.2}$$

where $\mathbf{n}$ is the outward normal to the surface and the stress tensor can be roughly interpreted as the distribution of force effects at each point. Now we use the divergence theorem on the surface integral, which relates the flux of a field (stress in this case) on a closed surface to the spatial divergence of that field within the volume, such that

$$\int_S \boldsymbol{\sigma}_{\mathrm{T}} \cdot \mathbf{n} \mathrm{d}S = \int_V \nabla_{\mathbf{x}} \boldsymbol{\sigma}_{\mathrm{T}} \mathrm{d}V, \tag{1.3}$$

where $\nabla_{\mathbf{x}}(\bullet)$ is the gradient operator of $\bullet$ with respect to the deformed position vector $\mathbf{x}$. We can eliminate the integration to get the following differential equation

$$\nabla_{\mathbf{x}} \boldsymbol{\sigma}_{\mathrm{T}} = \mathbf{0}. \tag{1.4}$$

FE software packages commonly use the weak form of differential equations. For example, using the principle of virtual work [Antman and Osborn, 1979], eq. (1.4) can be rewritten as

$$\int_V \nabla_{\mathbf{x}} \boldsymbol{\sigma}_{\mathrm{T}} \cdot \delta\mathbf{u} \mathrm{d}V = 0, \tag{1.5}$$

where $\delta\mathbf{u}$ denotes the virtual (non-zero) displacement field, which generates the virtual work. In practice, this variation simplifies the equation, as the result

of the integral is now a scalar value. Furthermore, using the integration by parts of this equation, the divergence theorem, and eq. (1.2), we can now directly impose the traction on the boundaries and remove the derivative term from the stress parameter [Holzapfel, 2000, Belytschko et al., 2014]:

$$\int_V \boldsymbol{\sigma}_{\mathrm{T}} : \nabla_{\mathbf{x}} \delta\mathbf{u} \mathrm{d}V - \int_S \mathbf{t} \cdot \delta\mathbf{u} \mathrm{d}S = 0. \tag{1.6}$$

Next, to account for the fluid contribution in cartilage load-bearing, we can use the continuity equation with the assumption that AC is a porous medium fully saturated with water. Thus,

$$\frac{\mathrm{d}}{\mathrm{d}t}\left(\int_V \rho\phi^{\mathrm{F}} \mathrm{d}V\right) + \int_S \rho\phi^{\mathrm{F}} \mathbf{n} \cdot \mathbf{v}_{\mathrm{r}} \mathrm{d}S = 0, \tag{1.7}$$

where ρ is the mass density of the fluid, $\mathbf{v}_{\mathrm{r}}$ is the relative velocity of the fluid with respect to the solid structure, and ϕ^{F} is the local volume fraction of the fluid. Conceptually, the first term models the rate of fluid change inside the tissue, whereas the second term reflects the amount crossing the boundary. Introducing the volume ratio J into the first term (to include the deformation of the solid structure) and applying the divergence theorem to the second term, the following partial differential equation is achieved

$$\frac{1}{J}\frac{\mathrm{d}}{\mathrm{d}t}\left(J\rho\phi^{\mathrm{F}}\right) + \nabla \cdot \left(\rho\phi^{\mathrm{F}}\mathbf{v}_{\mathrm{r}}\right) = 0. \tag{1.8}$$

The finite difference method can be used to approximate the temporal derivative by discretizing the time domain into time step Δt. In particular, the back-

ward Euler formula is used to approximate the temporal derivative of a function y by shifting the current time step one step forward and then applying the backward difference approximation according to

$$\left[\frac{\mathrm{d}y}{\mathrm{d}t}\right]_{t+\Delta t} \approx \frac{y_{t+\Delta t} - y_t}{\Delta t}. \tag{1.9}$$

Now, similar to the equilibrium equation, a weak form can be derived from eq. (1.8), and then the divergence theorem can be applied, yielding

$$\begin{aligned}\int_V \left(\left[\delta P\right]_{t+\Delta t} \left(\left[J\rho\phi^{\mathrm{F}}\right]_{t+\Delta t} - \left[J\rho\phi^{\mathrm{F}}\right]_t \right) - \Delta t \left[\rho\phi^{\mathrm{F}} \nabla_{\mathbf{x}} \delta P \cdot \mathbf{v}_{\mathrm{r}}\right]_{t+\Delta t} \right) \mathrm{d}V \\ + \Delta t \int_S \left[\delta P \rho\phi^{\mathrm{F}} \mathbf{n} \cdot \mathbf{v}_{\mathrm{r}}\right]_{t+\Delta t} \mathrm{d}S = 0,\end{aligned} \tag{1.10}$$

where δP is the virtual fluid pressure.

Next, FE methods are used to discretize the continuous spatial domain. For example, given a nonlinear 1D function $f(x)$, it can be approximated by $\bar{f}(x)$ as

$$\bar{f}(x) = \sum_{i=1}^{n} \sum_{j=1}^{2} \mathcal{N}_j^i(x) f(x_i). \tag{1.11}$$

Here, the geometrical domain is discretized into 1D FEs, where x_i is the nodal input value of the element i corresponding to the nodal result $f(x_i)$ with domain $[x_{i-1}, x_i]$, and $\mathcal{N}(x)$ is the shape function that can be defined by

$$\mathcal{N}_1^i(x) = \frac{x_i - x}{x_i - x_{i-1}} \qquad \text{and} \qquad \mathcal{N}_2^i(x) = \frac{x - x_{i-1}}{x_i - x_{i-1}}. \tag{1.12}$$

Conceptually, these particular shape functions approximate $f(x)$ as a group of

simpler linear functions connected with each other at their nodes. Likewise, by generalizing this to the 3D space with displacement and fluid pressure nodal values, the shape functions $\mathcal{N}^P$ and $\mathcal{N}^{\mathbf{u}}$ are defined to spatially discretize, respectively, P and $\mathbf{u}$ (and their virtual variations). Substituting them into eqs. (1.10) and (1.6) results in

$$\mathcal{F} = 0, \tag{1.13}$$

where, $\mathcal{F} = [\mathcal{F}_1, \mathcal{F}_2]^{\mathrm{T}}$ with

$$\mathcal{F}_1 = \int_V \left[\boldsymbol{\sigma} : \nabla_{\mathbf{x}} \mathcal{N}^{\mathbf{u}}\right]_{t+\Delta t} \mathrm{d}V - \int_S \left[\mathbf{t} \cdot \mathcal{N}^{\mathbf{u}}\right]_{t+\Delta t} \mathrm{d}S, \tag{1.14}$$

$$\begin{aligned} \mathcal{F}_2 \;=\; & \int_V \left(\mathcal{N}^p_{t+\Delta t} \left(\left[J\rho\phi^F\right]_{t+\Delta t} - \left[J\rho\phi^F\right]_t\right) - \Delta t \left[\rho\phi^F \nabla_{\mathbf{x}} \mathcal{N}^p \cdot \mathbf{v}_{\mathrm{r}}\right]_{t+\Delta t}\right) \mathrm{d}V \\ & + \Delta t \int_S \left[\mathcal{N}^p \rho\phi^F \mathbf{n} \cdot \mathbf{v}_{\mathrm{r}}\right]_{t+\Delta t} \mathrm{d}S = 0. \end{aligned} \tag{1.15}$$

This discretization technique is referred to as implicit FE modeling because it provides a set of equations between the unknown parameters at the end of time step $t + \Delta t$ and the known parameters at step t (obviously once the discretized constitutive equations and additional conditions have been applied). Due to the high stability of this method, well-established software packages such as Abaqus use similar formulations. However, the existence of a nonlinear system of equations requires the use of a root-finding technique such as Newton's method [Almeida and Spilker, 1997, Belytschko et al., 2014].

We denote $\mathfrak{U}$ as the vector of system variables, such as $\{u_1, u_2, u_3, P\}$, where $u_1,\ u_2$, and u_3 correspond to the components of $\mathbf{u}$ in the 3D Cartesian coordinate system. To linearize eq. (1.13), Newton's method uses the Jacobian matrix $\mathfrak{J}^{(i)}$ at each iteration i, i.e.

$$\mathfrak{J}^{(i)} = \begin{bmatrix} \frac{\partial \mathcal{F}_1^{(i)}}{\partial u_1^{(i)}} & \cdots & \frac{\partial \mathcal{F}_1^{(i)}}{\partial P^{(i)}} \\ \frac{\partial \mathcal{F}_2^{(i)}}{\partial u_1^{(i)}} & \cdots & \frac{\partial \mathcal{F}_2^{(i)}}{\partial P^{(i)}} \end{bmatrix}, \tag{1.16}$$

where

$$\mathcal{F}^{(i)} = \mathcal{F}\Big|_{\mathfrak{U}^t = \mathfrak{U}^{(i-1)},\ \mathfrak{U}^{t+\Delta t} = \mathfrak{U}^{(i)}}, \tag{1.17}$$

assuming that $i \in \mathbb{N}$ and $\mathfrak{U}^{(0)}$ is the previously known value of $\mathfrak{U}$ at the beginning of the increment (i.e., the values that have been computed from the previous increment or the initial state). In this manner, it linearizes the nonlinear equations iteratively with an initial guess $\mathfrak{U}^{(1)}$, i.e.

$$\mathcal{F}^{(i+1)} = \mathcal{F}^{(i)} + \left(\mathfrak{U}^{(i+1)} - \mathfrak{U}^{(i)}\right) \cdot \mathfrak{J}^{(i)}. \tag{1.18}$$

To solve this problem, at each step the integrations in the discretized equations for each FE are calculated (typically with numerical approximation), resulting in a set of linear equations. These equations can then be solved either directly or iteratively using well-established techniques in linear algebra, thereby determining $\mathfrak{U}^{(i+1)}$. This process is assumed converged once $\left(\mathcal{F}^{(i+1)}\right)^2$ becomes sufficiently small, indicating that eq. (1.13) is approximately solved and the unknown parameters are estimated at step $t + \Delta t$. This is an extremely simplified representation of the numerical modeling, which can give an overall

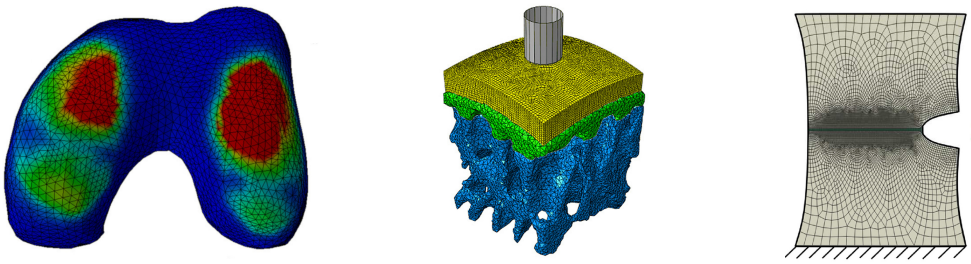

Figure 1.3: Examples of finite element studies, showing that element shapes depend on the geometric complexity and physics problems. The image has been modified from Orava et al. [2022], Orozco et al. [2022] and Ardatov et al. [2023] under their CC BY 4.0 license, permitting reuse with a proper citation.

understanding of the solution procedure and its highly iterative nature [Belytschko et al., 2014]. Furthermore, the exact definition of the shape functions may vary depending on the specific physics problem, e.g., the existence of contact mechanics and geometric complexity (Figure 1.3). Some implementations may use more advanced linearization techniques or apply an explicit FE method [Almeida and Spilker, 1997, Korsawe et al., 2006, Nakahara et al., 2016]. But regardless of these differences, they are still developed based on similar iterative algorithms, which explains why they can be expensive to run.

1.3.2. Constitutive modeling

We first introduce the tensors that are often used in constitutive modeling of nonlinear materials [Holzapfel, 2000]. Suppose $\nabla_{\mathbf{X}}(\bullet)$ is the gradient operator of $\bullet$ with respect to the vector of undeformed position $\mathbf{X}$ and $\mathbf{I}$ is the identity

tensor, the deformation gradient $\mathbf{F}$ is calculated as

$$\mathbf{F} = \mathbf{I} + \nabla_{\mathbf{X}}\mathbf{u}. \tag{1.19}$$

This is a measure of the relative deformation, formulated by a second-order tensor, which can be decomposed into an orthogonal tensor (i.e., the rotation tensor $\mathbf{R}$) and a positive definite symmetric tensor (i.e., the left stretch tensor $\mathbf{V}$), i.e.

$$\mathbf{F} = \mathbf{V}\mathbf{R}. \tag{1.20}$$

This equation allows us to focus only on the stretch in the tissue (which is responsible for the stress response of the tissue in AC analyses), since $\mathbf{R}^{\mathrm{T}}\mathbf{R} = \mathbf{I}$. The left Cauchy-Green tensor $\mathbf{B}$ is thus defined in such a way to exclude the effect of rigid body rotation. For this reason,

$$\mathbf{B} = \mathbf{F}\mathbf{F}^{\mathrm{T}} = \mathbf{V}^2. \tag{1.21}$$

These tensors can be associated with the volume ratio by

$$J = \sqrt{\det \mathbf{B}} = \det \mathbf{F} > 0. \tag{1.22}$$

With anisotropic materials, it is imperative to include the direction dependency in their equations. For example, the direction of the fibril bundle I is given by the unit direction vector $\mathbf{N}^I$, which can change to its new unit direction $\mathbf{n}^I$ after deformation. It can be calculated by first deforming the initial direction

vector (using the deformation gradient) and then scaling it to its unit size, i.e.

$$\mathbf{n}^I = \frac{\mathbf{F}\mathbf{N}^I}{\|\mathbf{F}\mathbf{N}^I\|_2}, \tag{1.23}$$

where $\|\bullet\|_2$ denotes the l^2 norm of $\bullet$. Instead of considering the entire deformation, we can now focus on the deformation in the specific direction of the fibrils using the logarithmic strain ϵ^I in the direction of the deformed bundles (as a measure of the large deformation). Thus,

$$\epsilon^I = \log(\lambda^I), \tag{1.24}$$

where λ^I is the fibrillar stretch, which can be correlated with the total deformation using finite strain theory, i.e.

$$\lambda^I = \sqrt{\mathbf{n}^I \cdot \mathbf{B} \cdot \mathbf{n}^I}. \tag{1.25}$$

Now, the solid-fluid interaction is modeled using the classical porous media theory and Darcy's law, stating that the fluid flows from a region of higher pressure to lower pressure, and the rate of that depends on the material properties [Terzaghi, 1943, Dullien, 1979]. Thus,

$$\phi^F \mathbf{v}_{\mathrm{r}} = -\frac{1}{\mu}\mathbf{K} \cdot \nabla_{\mathbf{x}} P, \tag{1.26}$$

where μ is the dynamic viscosity (the internal flow resistance of the fluid) and $\mathbf{K}$ is the permeability tensor (the ability to transmit fluids through the porous

structure). In addition, the stress caused by this pressure together with the effective stress tensor $\boldsymbol{\sigma}^{\mathrm{EFF}}$ (that transmits to the solid structure) determines the total stress $\boldsymbol{\sigma}_{\mathrm{T}}$ as

$$\boldsymbol{\sigma}_{\mathrm{T}} = \boldsymbol{\sigma}^{\mathrm{EFF}} - P\mathbf{I}. \tag{1.27}$$

By defining the constitutive behavior of the solid structure and its relationship with tissue deformation, eq. (1.27) is fully determined. Once this equation and eq. (1.26) are discretized (as explained in the previous section), they can be introduced into the governing equation, eq. (1.13), to replace the relative velocity and stress tensor. Regardless of this, the inclusion of advanced multi-physics constitutive models of AC might make this process even more iterative. This is explained here by exemplifying one of the most up-to-date multiphasic cartilage models [Sajjadinia et al., 2021a].

The constrained mixture theory is used [Klisch, 1999], which is arguably the most popular constitutive multi-physics model to define the effective stress in AC. It assumes the non-fluid phases are confined together and have a similar deformation, yielding

$$\boldsymbol{\sigma}^{\mathrm{EFF}} = \boldsymbol{\sigma}^{\mathrm{COL}} + \boldsymbol{\sigma}^{\mathrm{MAT}} - \boldsymbol{\sigma}^{\mathrm{GAG}}. \tag{1.28}$$

Here the superscripts COL, MAT, and GAG denote the contributions of the fibrillar collagen network, the non-fibrillar extracellular matrix, and the osmotic pressure, respectively [Mow et al., 1980, Wilson et al., 2005, Sajjadinia et al., 2019].

Regarding the collagen fibrils, it is experimentally observed that they bear

loads nonlinearly correlated with their strains [Charlebois et al., 2004], e.g., by $(E_1 + E_2\epsilon^I)\epsilon^I$, where E_1 and E_2 signify the degree of nonlinearity. This response, before application to its constitutive equation, needs two modifications: (i) multiplication by λ^I/J, the inverse of the fibril bundle surface area, to account for surface area effects; and (ii) multiplication by the components' volume fractions, reflecting each component's contribution according to the mixture theory. Thus, the tensile stress in each fibril bundle σ^I can be evaluated as follows [Wilson et al., 2007, Sajjadinia et al., 2019]

$$\sigma^I = \phi_0^{\mathrm{S}} \rho_{\mathrm{C}}^I \frac{\lambda^I}{J}(E_1 + E_2\epsilon^I)\epsilon^I, \tag{1.29}$$

where ρ_{C}^I is the volume fraction of the relevant fibrils and ϕ_0^{S} is the initial value of the solid volume fraction. Then the stress in the collagen fibril network $\boldsymbol{\sigma}^{\mathrm{COL}}$ can be defined considering the contributions of all fibrils [Wilson et al., 2004], i.e.

$$\boldsymbol{\sigma}^{\mathrm{COL}} = \sum_{I=1}^{9} \sigma^I \mathbf{n}^I \otimes \mathbf{n}^I, \tag{1.30}$$

where $\otimes$ denotes the dyadic product. This summation takes into account the orientations of all bundles (as explained in Section 1.2.2) and their stress contributions.

Next, the osmotic pressure can be defined by first deriving a model for glycosaminoglycan-related electrostatic force and then simplifying it by relating this force only to the deformation in the solid matrix [Ateshian et al., 2004]. This can lead to an exponential form of the osmotic stress contribution via two positive material constants, i.e. α_1 and α_2 [Buschmann and Grodzin-

sky, 1995, Stender et al., 2013], i.e.

$$\boldsymbol{\sigma}^{\mathrm{GAG}} = \alpha_1 J^{-\alpha_2}\mathbf{I}. \tag{1.31}$$

The other components of the solid phase are usually represented by an isotropic nonlinear elastic model, e.g., using one of the popular neo-Hookean equations, formulated on the basis of the thermodynamics of rubber-like materials, see, e.g., Kim et al. [2012]. This model is modified to consider the effects of the volume fractions of the material [Wilson et al., 2007, Sajjadinia et al., 2021a], i.e.

$$\begin{aligned}\boldsymbol{\sigma}^{\mathrm{MAT}} \;=\; & \phi_0^{\mathrm{S}} G_m \frac{1-\rho_0^{\mathrm{COL}}}{J}\left[-\frac{\ln J}{6}\left(3\phi_0^{\mathrm{S}}\frac{J\ln J}{(J-\phi_0^{\mathrm{S}})^2}\right.\right.\\ & \left.\left.-1-3\frac{J+\phi_0^{\mathrm{S}}}{J-\phi_0^{\mathrm{S}}}\right)\mathbf{I}+(\mathbf{B}-J^{2/3}\mathbf{I})\right],\end{aligned} \tag{1.32}$$

where G_m is an additional material constant and ρ_0^{COL} is the initial value of the total collagen volume fraction ρ^{COL}. The volume fractions are updated by the continuity equation of the solid phases as

$$\varphi = \frac{\varphi_0}{J} \qquad \varphi \in \left\{\phi^{\mathrm{S}},\ \rho^{\mathrm{COL}}\right\}. \tag{1.33}$$

While the above-mentioned equations formulate the constitute behavior for FE analysis of cartilage, due to the fixed charges in this tissue, the *in vivo* data recorded in the literature mostly consider the pre-stressed state as the initial condition. This is in contrast to mathematical models, which typically consider the stress-free state as the initial state, resulting in a large discrepancy

between the initial numerical conditions and the *in vivo* conditions. The pre-stress $\boldsymbol{\sigma}_0$ can be verified by setting $\mathbf{F} = \mathbf{I}$ (which only applies the initial boundary conditions), i.e.

$$\boldsymbol{\sigma}_0 = -\alpha \mathbf{I}. \tag{1.34}$$

This causes the tissue to swell until it reaches equilibrium (as mentioned in Section 1.2.2). This can then change the initial geometrical properties and material fractions, e.g., according to eq. (1.33). Therefore, the numerical solvers should first find the pre-stressed state (observable as *in vivo*) by starting from the unknown stress-free state. The initial state can be approximated using a pre-stressing algorithm, which is essentially an optimization algorithm that employs multiple FE analyses to test various stress-free states and identify the approximate stress-free states [Wang et al., 2018, Sajjadinia et al., 2021a]. The application of this algorithm makes the numerical simulation more iterative, which may be alleviated by ML, as briefly discussed in the following section.

1.4. AI-Enhanced Modeling

1.4.1. Deep learning

Assuming $\mathcal{X}$ and $\mathcal{Y}$ are the sets of corresponding measurable spaces, supervised ML is the task of constructing a model function f that can ideally map each element of input data $\mathcal{X}$ to its corresponding member in the output set $\mathcal{Y}$ according to

$$f : \mathcal{X} \longrightarrow \mathcal{Y}. \tag{1.35}$$

The output examples, used for generation and evaluation of the model, known as labels, are typically obtained by human or systemic supervision. Each input-output pair of samples can be characterized by multidimensional quantitative properties (or features). For example, in a pre-stressing simulation, the known pre-stressed geometry, physical constraints, and constitutive parameters can be used as input features, while the labels can be the observed or numerically calculated stress-free states.

Given a subset of labeled data $\mathcal{Z} \subset \mathcal{X} \times \mathcal{Y}$, a learning algorithm, especially in the context of deep learning, finds the best function f, using the errors measured by a loss function $\mathcal{L}$, i.e.

$$\mathcal{L} : \mathcal{M}\left(\mathcal{X}, \mathcal{Y}\right) \times \mathcal{Z} \longrightarrow \mathbb{R}, \tag{1.36}$$

where $\mathcal{M}\left(\mathcal{X}, \mathcal{Y}\right)$ is the set of possible measurable and learnable functions with different hypothetical architectures, such as artificial neural networks [Abiodun et al., 2019]. In the basic multi-layer feed-forward neural network (FFNN) with fully connected or dense layers [Rumelhart et al., 1986], the sequence of input features (i.e., the input layer) is connected to its subsequent layer. The data derived from the previous layers provide the input signals of the next layer up to the very last output layer (generation of the output data). Assuming such an FFNN model represented by $\Psi \in \mathcal{M}\left(\mathcal{X}, \mathcal{Y}\right)$, then

$$\Psi(x;\ \cdot, \Theta) = \psi^{(L)}\left(\psi^{(L-1)}\left(\cdots\left(\psi^{(1)}\left(\psi^{(0)}\left(x\right)\right)\right)\right)\right). \tag{1.37}$$

Here, $\psi^{(i)}$ is a transformation through the layer $i \in [0, L]$, with the assumption

that layer 0 is the input layer, i.e., $\psi^{(0)}(x) = x$. Also, Θ (the set of trainable parameters) and hyperparameters (like the number of layers) define the exact definition of each layer $\psi^{(i)}$. For most regression problems, the basic definition of $\psi^{(i)}$ is as follows

$$\psi^{(i)}(x) = \begin{cases} W^{(i)}\psi^{(i-1)}(x) + b^{(i)} & \text{if } i = L, \\ a\left(W^{(i)}\psi^{(i-1)}(x) + b^{(i)}\right) & \text{others,} \end{cases} \tag{1.38}$$

where W and b are respectively the trainable weight and bias parameters (finding the best linear combination), and a is the activation function, which nonlinearly amplifies or attenuates the effects of the input signals to help capture nonlinear patterns [Berner et al., 2022]. An efficient activation function is the rectified linear unit function, which is basically a ramp function that ignores the negative signals [Fukushima, 1980, Nair and Hinton, 2010], i.e.,

$$a(x) = \max(0,\ x). \tag{1.39}$$

During training, an initial guess of the trainable parameters is first made, which may result in some errors in the generated output data compared to the labels. This error can then be minimized by using an optimization algorithm that iteratively changes the trainable parameters until the most accurate and generalizable model is achieved.

The algorithm has undergone significant enhancements, most notably the integration of normalization layers, which stabilize the training of models by normalizing different distributions of input signals [Bianchi et al., 2012, Sali-

mans and Kingma, 2016, Bjorck et al., 2018, Xu et al., 2019]. This allows implementation of neural networks with many hidden layers to tackle complex problems. In addition, specialized variations have been developed to cater to distinct data structures: recurrent neural networks [Yu et al., 2019] and transformers [Lin et al., 2022] for temporal information, and convolutional neural networks [Ajit et al., 2020] for spatial information. A challenge, however, is the lack of permutation invariance in these algorithms. This means the order of features is relevant, which becomes problematic with FE nodal data, where the order of nodal features to be considered is usually of no importance [Géron, 2019].

In this regard, message-passing graph neural networks (MPGNNs) have two key benefits: their ability to maintain permutation invariance and to efficiently process varying numbers of nodes. The salient feature of MPGNNs is their focus on individual nodes and their connections to neighboring nodes rather than the entire mesh. Given a node n with feature vector denoted by $\mathfrak{v}_n$, the set $\Gamma(n)$ of its neighboring nodes is derived from the mesh topology, i.e., the nodal connections. Subsequently, information about the neighbors is aggregated using an aggregation function, such as a sum function, to be further processed by an FFNN, i.e.

$$\mathfrak{v}'_n = \text{FFNN}\left(\sum_{i\in\Gamma(n)} \mathfrak{v}_i, \mathfrak{v}_n\right), \tag{1.40}$$

where $\mathfrak{v}'_n$ is the updated nodal representation. An enrichment of global information is possible by increasing the number of sequentially message-passing

layers connected to one another. Despite the versatility of this method, it can be enhanced further through variations, e.g., by assigning features to each connection, i.e., edge features defined by different distance metrics to account for the nodal geometrical information. This approach eliminates the need to directly encode nodal positions as nodal features and allows spatial equivariance in the surrogate [Cai et al., 2018, Zhou et al., 2020, Wu et al., 2021].

Incorporating edge features or other types of features may alter the aggregation functions applied to each entity, such as the node and the edge, thus potentially changing eq. (1.40). However, the underlying concepts remain the same: the mesh data is initially converted into a graph, and two FFNNs update each node or edge feature after aggregating the neighboring features. Consequently, a transformed graph representation is generated that facilitates learning by isolating highly local data. This process can be reiterated with further message passing until it reaches the output layer, yielding nodal outputs [Sperduti and Starita, 1997, Battaglia et al., 2018, Riba et al., 2018].

1.4.2. Surrogate modeling

Training the surrogates of cartilage models by supervised ML requires a set of data samples generated from a high-fidelity numerical model, as discussed in Section 1.3, which may become prohibitively expensive. Therefore, typical FFNNs were trained on the data generated from simplified FE models, e.g., Paiva et al. [2012] used a surrogate for their multiscale cartilage simulation but using a very simplified elastic model (ignoring the nonlinear multi-physics).

Arbabi et al. [2016a] included the biphasic equations in their surrogate of a 2D cartilage model, but ignored the vital osmotic pressure. Arbabi et al. [2016b] then managed to use a multi-physics model to train the surrogate, but with $10\,000$ samples.

Under specific conditions, such as reducing the scale of the simulation, a surrogate may be generated with only a few samples (see, e.g., [Faisal et al., 2023]). However, for complex multi-physics equations, particularly in large-scale and high-dimensional data, having a large training dataset becomes unavoidable. If the primary purpose of applying ML is to enhance efficiency, the models should ideally be trained on a limited number of samples, especially when the numerical generation of these samples is costly [Forrester et al., 2008]. This factor often leads to the underutilization of AI-enhanced modeling techniques.

Our research group recently developed a specialized hybrid ML algorithm [Sajjadinia et al., 2022] that can be trained on very small datasets of the multi-physics models of soft tissues, especially cartilage-like materials. The key idea is to insert a simplified version of the numerical model into the surrogate model by ignoring some of the physical behaviors of the high-fidelity model, e.g., some of the constitutive equations, to create a dataset with low-fidelity but inexpensive samples. The ML model then finds a mapping between the low-fidelity and high-fidelity data, and therefore the high-fidelity model is only used for training. The low-fidelity numerical model used in the surrogate transforms the input features into more informative features, i.e., an approximation of the high-fidelity results that can significantly improve the training

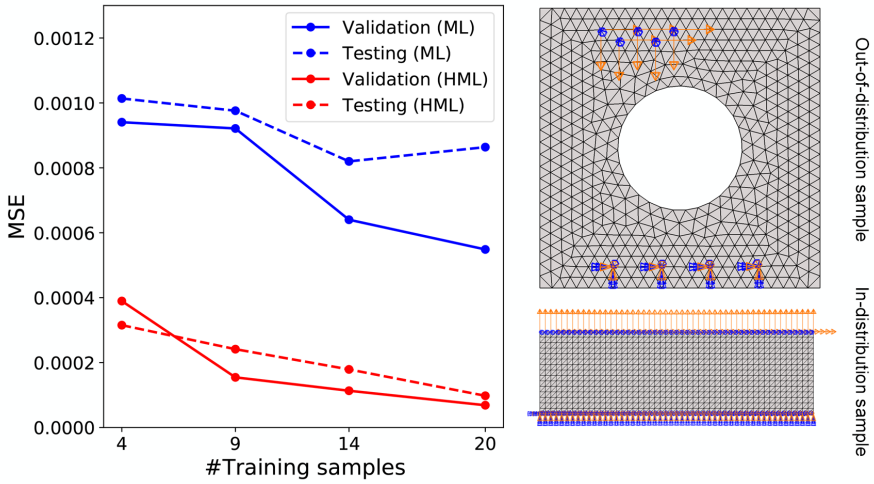

Figure 1.4: Examples of 2D in-distribution and out-of-distribution models used in the validation and test sets (right) and the corresponding plot of the trained surrogate errors in these sets versus the number of training samples (left). The image has been modified from Sajjadinia et al. [2022] under its CC BY 4.0 license, permitting reuse with a proper citation. Abbreviation: MSE = mean squared error; ML = machine learning; HML = hybrid machine learning.

performance with small datasets. This has been shown experimentally by 2D and 3D simulations.

The 2D simulations, shown in Figure 1.4, chose a multi-physics model with and without pre-stressing optimizers for the low-fidelity and high-fidelity models, respectively, on two sets of in-distribution validation samples and out-of-distribution test samples (to also assess the generalizability of the surrogates). The results indicate that the hybrid ML model can outperform the ML surrogates with only four samples (using the MPGNNs that allow generalizable inference). Likewise, through pointwise evaluation [Sajjadinia et al., 2021b], we observed similar performance improvements in another 3D model in that study. The latency (run-time after training) of this model was relatively

2 to 14 times smaller, even though the numerical model had been simplified for fast data generation.

While specialized surrogate models are not commonly applied in AC modeling, likely due to the complexity of implementing numerical models, previous studies have successfully used multi-fidelity approaches with different hybrid or full ML surrogates. These approaches have yielded comparable performance improvements in other application domains. Traditional ML techniques such as Gaussian processes have predominantly been used [Cheng et al., 2021, Zhang et al., 2022], while advanced physics problems are often implemented using different neural network architectures [Yang and Perdikaris, 2019, Ahn et al., 2022]. With these promising results, multi-fidelity and hybrid surrogates are expected to further advance in the biomechanical modeling of AC.

1.5. Discussion and Conclusion

This chapter has provided an overview of biomechanical modeling methods enhanced with AI that perform advanced numerical simulations using ML surrogates. Focusing on the biomechanical constitutive modeling of cartilage, we first reviewed the main load-bearing components of AC (to be included in the high-fidelity simulations) and then we elaborated on the constitutive equations to demonstrate the complexity of such models. In particular, it was pointed out that these models are commonly implemented through advanced multi-physics equations and iterative numerical algorithms, making their data generation too time-consuming. We have tried to clarify that ML surrogates may solve this problem, especially when implemented by the multi-fidelity and hybrid ML

algorithms.

The hybrid ML implementations showed encouraging results as they could be trained with fewer samples compared to the regular ML counterparts. However, they were only tested on simplified numerical models, and the important collagen fibrils were neglected. Therefore, an interesting research direction for future studies is to evaluate such hybrid methods using all major biomechanical components of cartilage. This raises further questions regarding the exact learning and numerical methods that can find the best compromise between the performance and computational efforts for different simulation tasks.

In summary, the contribution of hybrid surrogates to AC modeling can be seen as an example of the meaningful application of AI in biomechanical simulation or more generally in the field of *in silico* biomedicine.

Bibliography

Abaqus. Dassault systèmes Simulia corp., providence, RI, USA. URL http://www.simulia.com.

O.I. Abiodun, A. Jantan, A.E. Omolara, et al. Comprehensive review of artificial neural network applications to pattern recognition. *IEEE Access*, 7:158820–158846, 2019. URL https://doi.org/10.1109/ACCESS.2019.2945545.

J.G. Ahn, H.I. Yang, and J.G. Kim. Multi-fidelity meta modeling using composite neural network with online adaptive basis technique. *Computer*

Methods in Applied Mechanics and Engineering, 388:114258, 2022. ISSN 0045-7825. URL https://doi.org/10.1016/j.cma.2021.114258.

A. Ajit, K. Acharya, and A. Samanta. A review of convolutional neural networks. In *2020 International Conference on Emerging Trends in Information Technology and Engineering (ic-ETITE)*, pages 1–5, 2020. URL https://doi.org/10.1109/ic-ETITE47903.2020.049.

E.S. Almeida and R.L. Spilker. Mixed and penalty finite element models for the nonlinear behavior of biphasic soft tissues in finite deformation: Part I—alternate formulations. *Computer Methods in Biomechanics and Biomedical Engineering*, 1(1):25–46, 1997. URL https://doi.org/10.1080/01495739708936693.

M. Alunni Cardinali, M. Govoni, M. Tschon, et al. Brillouin–Raman microspectroscopy and machine learning techniques to classify osteoarthritic lesions in the human articular cartilage. *Scientific Reports*, 13(1):1690, 2023. ISSN 2045-2322. URL https://doi.org/10.1038/s41598-023-28735-5.

S. S. Antman and J. E. Osborn. The principle of virtual work and integral laws of motion. *Archive for Rational Mechanics and Analysis*, 69(3):231–262, 1979. ISSN 1432-0673. URL https://doi.org/10.1007/BF00248135.

V. Arbabi, B. Pouran, G. Campoli, et al. Determination of the mechanical and physical properties of cartilage by coupling poroelastic-based finite element models of indentation with artificial neural networks. *Jour-*

nal of Biomechanics, 49(5):631–637, 2016a. ISSN 0021-9290. URL https://doi.org/10.1016/j.jbiomech.2015.12.014.

V. Arbabi, B. Pouran, H. Weinans, et al. Combined inverse-forward artificial neural networks for fast and accurate estimation of the diffusion coefficients of cartilage based on multi-physics models. *Journal of Biomechanics*, 49 (13):2799–2805, 2016b. ISSN 0021-9290. URL https://doi.org/10.1016/j.jbiomech.2016.06.019.

O. Ardatov, V. Aleksiuk, A. Maknickas, et al. Modeling the impact of meniscal tears on von Mises stress of knee cartilage tissue. *Bioengineering*, 10(3), 2023. ISSN 2306-5354. URL https://doi.org/10.3390/bioengineering10030314.

J. L. Astephen Wilson and D. Kobsar. Osteoarthritis year in review 2020: Mechanics. *Osteoarthritis and Cartilage*, 29(2):161–169, 2021. ISSN 1063-4584. URL https://doi.org/10.1016/j.joca.2020.12.009.

G.A. Ateshian, N.O. Chahine, I.M. Basalo, et al. The correspondence between equilibrium biphasic and triphasic material properties in mixture models of articular cartilage. *Journal of Biomechanics*, 37(3):391–400, 2004. ISSN 0021-9290. URL https://doi.org/10.1016/S0021-9290(03)00252-5.

H.T. Banks, S. Hu, and Z.R. Kenz. A brief review of elasticity and viscoelasticity for solids. *Advances in Applied Mathematics and Mechanics*, 3(1): 1–51, 2011. URL https://doi.org/10.4208/aamm.10-m1030.

P.W. Battaglia, J.B. Hamrick, V. Bapst, et al. Relational inductive biases, deep

learning, and graph networks, 2018. URL https://doi.org/10.48550/arxiv.1806.01261.

T. Belytschko, W.K. Liu, B. Moran, et al. *Nonlinear Finite Elements for Continua and Structures*. John Wiley & Sons, 2014.

J. Berner, P. Grohs, G. Kutyniok, et al. The modern mathematics of deep learning. In P. Grohs and G. Kutyniok, editors, *Mathematical Aspects of Deep Learning*, page 1–111. Cambridge University Press, 2022. URL https://doi.org/10.1017/9781009025096.002.

M. Bianchi, G. Kassay, and R. Pini. Conditioning for optimization problems under general perturbations. *Nonlinear Analysis: Theory, Methods & Applications*, 75(1):37–45, 2012. ISSN 0362-546X. URL https://doi.org/10.1016/j.na.2011.07.061.

B.J. Bielajew, J.C. Hu, and K.A. Athanasiou. Collagen: Quantification, biomechanics and role of minor subtypes in cartilage. *Nature Reviews Materials*, 5(10):730–747, 2020. ISSN 2058-8437. URL https://doi.org/10.1038/s41578-020-0213-1.

N. Bjorck, C.P. Gomes, B. Selman, et al. Understanding batch normalization. In S. Bengio, H. Wallach, H. Larochelle, et al., editors, *Advances in Neural Information Processing Systems*, volume 31. Curran Associates, Inc., 2018. URL https://proceedings.neurips.cc/paper/2018/file/36072923bfc3cf47745d704feb489480-Paper.pdf.

L. Bozec, G. van der Heijden, and M. Horton. Collagen fibrils: Nanoscale

ropes. *Biophysical Journal*, 92(1):70–75, 2007. ISSN 0006-3495. URL https://doi.org/10.1529/biophysj.106.085704.

L.T. Brody. Knee osteoarthritis: Clinical connections to articular cartilage structure and function. *Physical Therapy in Sport*, 16(4):301–316, 2015. ISSN 1466-853X. URL https://doi.org/10.1016/j.ptsp.2014.12.001.

J.A. Buckwalter. Osteoarthritis and articular cartilage use, disuse, and abuse: Experimental studies. *The Journal of Rheumatology. Supplement*, 43:13–15, 1995. ISSN 0380-0903. URL http://europepmc.org/abstract/MED/7752117.

M.D. Buschmann and A.J. Grodzinsky. A molecular model of proteoglycan-associated electrostatic forces in cartilage mechanics. *Journal of Biomechanical Engineering*, 117(2):179–192, 1995. ISSN 0148-0731. doi: 10.1115/1.2796000. URL https://doi.org/10.1115/1.2796000.

H. Cai, V.W. Zheng, and K.C. Chang. A comprehensive survey of graph embedding: Problems, techniques, and applications. *IEEE Transactions on Knowledge and Data Engineering*, 30(9):1616–1637, 2018. URL https://doi.org/10.1109/TKDE.2018.2807452.

A.A. Cederlund and R.M. Aspden. Walking on water: Revisiting the role of water in articular cartilage biomechanics in relation to tissue engineering and regenerative medicine. *Journal of The Royal Society Interface*, 19(193): 20220364, 2022. URL https://doi.org/10.1098/rsif.2022.0364.

M. Charlebois, M.D. McKee, and M.D. Buschmann. Nonlinear tensile properties of bovine articular cartilage and their variation with age and depth. *Journal of Biomechanical Engineering*, 126(2):129–137, 2004. ISSN 0148-0731. URL https://doi.org/10.1115/1.1688771.

A. Chen, C. Gupte, and K. Akhtar. The global economic cost of osteoarthritis: How the UK compares. *Arthritis*, 2012:698709, 2012. ISSN 2090-1984. URL https://doi.org/10.1155/2012/698709.

S. Chen, P. Fu, H. Wu, et al. Meniscus, articular cartilage and nucleus pulposus: A comparative review of cartilage-like tissues in anatomy, development and function. *Cell and Tissue Research*, 370(1):53–70, 2017. ISSN 1432-0878. URL https://doi.org/10.1007/s00441-017-2613-0.

M. Cheng, P. Jiang, J. Hu, et al. A multi-fidelity surrogate modeling method based on variance-weighted sum for the fusion of multiple non-hierarchical low-fidelity data. *Structural and Multidisciplinary Optimization*, 64(6):3797–3818, 2021. ISSN 1615-1488. URL https://doi.org/10.1007/s00158-021-03055-2.

J.M. Clark. The organization of collagen in cryofractured rabbit articular cartilage: A scanning electron microscopic study. *Journal of Orthopaedic Research*, 3(1):17–29, 1985. URL https://doi.org/10.1002/jor.1100030102.

M.E. Cooke, B.M. Lawless, S.W. Jones, et al. Matrix degradation in osteoarthritis primes the superficial region of cartilage for mechanical dam-

age. *Acta Biomaterialia*, 78:320–328, 2018. ISSN 1742-7061. URL https://doi.org/10.1016/j.actbio.2018.07.037.

R.J. Cooper, R.K. Wilcox, and A.C. Jones. Finite element models of the tibiofemoral joint: A review of validation approaches and modelling challenges. *Medical Engineering & Physics*, 74:1–12, 2019. ISSN 1350-4533. URL https://doi.org/10.1016/j.medengphy.2019.08.002.

E.M. Culav, C.H. Clark, and M.J. Merrilees. Connective tissues: Matrix composition and its relevance to physical therapy. *Physical Therapy*, 79(3):308–319, 1999. ISSN 0031-9023. URL https://doi.org/10.1093/ptj/79.3.308.

E.K. Danso, J.T.J. Honkanen, S. Saarakkala, et al. Comparison of nonlinear mechanical properties of bovine articular cartilage and meniscus. *Journal of Biomechanics*, 47(1):200–206, 2014. ISSN 0021-9290. URL https://doi.org/10.1016/j.jbiomech.2013.09.015.

J. Dudhia. Aggrecan, aging and assembly in articular cartilage. *Cellular and Molecular Life Sciences CMLS*, 62(19):2241–2256, 2005. ISSN 1420-9071. URL https://doi.org/10.1007/s00018-005-5217-x.

F.A.L. Dullien. *Porous Media: Fluid Transport and Pore Structure*. Elsevier Science, 1979.

S.F. Dye. An evolutionary perspective of the knee. *The Journal of Bone and Joint Surgery. American volume*, 69(7):976–983, 1987. ISSN 0021-9355. URL http://europepmc.org/abstract/MED/3654710.

M. Ebrahimi, S. Ojanen, A. Mohammadi, et al. Elastic, viscoelastic and fibril-reinforced poroelastic material properties of healthy and osteoarthritic human tibial cartilage. *Annals of Biomedical Engineering*, 47(4):953–966, 2019. ISSN 1573-9686. URL https://doi.org/10.1007/s10439-019-02213-4.

F.S. Egli, R.C. Straube, A. Mielke, et al. Surrogate modeling of a nonlinear, biphasic model of articular cartilage with artificial neural networks. *PAMM*, 21(1):e202100188, 2021. URL https://doi.org/10.1002/pamm.202100188.

J. Eschweiler, N. Horn, B. Rath, et al. The biomechanics of cartilage—an overview. *Life*, 11(4), 2021. ISSN 2075-1729. URL https://doi.org/10.3390/life11040302.

T.R. Faisal, M. Adouni, and Y.Y. Dhaher. Surrogate modeling of articular cartilage degradation to understand the synergistic role of MMP-1 and MMP-9: A case study. *Biomechanics and Modeling in Mechanobiology*, 22(1):43–56, 2023. ISSN 1617-7940. URL https://doi.org/10.1007/s10237-022-01630-0.

A.I.J. Forrester, A. Sóbester, and A.J. Keane. *Engineering Design via Surrogate Modelling*. Wiley, 2008. URL https://doi.org/10.1002/9780470770801.

H. Forster and J. Fisher. The influence of loading time and lubricant on the friction of articular cartilage. *Proceedings of the Institution of Mechanical*

Engineers, Part H: Journal of Engineering in Medicine, 210(2):109–119, 1996. URL https://doi.org/10.1243/PIME_PROC_1996_210_399_02.

M. Freutel, H. Schmidt, L. Dürselen, et al. Finite element modeling of soft tissues: Material models, tissue interaction and challenges. *Clinical Biomechanics*, 29(4):363–372, 2014. ISSN 0268-0033. URL https://doi.org/10.1016/j.clinbiomech.2014.01.006.

K. Fukushima. Neocognitron: A self-organizing neural network model for a mechanism of pattern recognition unaffected by shift in position. *Biological Cybernetics*, 36(4):193–202, 1980. ISSN 1432-0770. URL https://doi.org/10.1007/BF00344251.

A. Géron. *Hands-On Machine Learning with Scikit-Learn, Keras, and TensorFlow: Concepts, Tools, and Techniques to Build Intelligent Systems*. O'Reilly Media, Inc., 2nd edition, 2019. ISBN 9781492032649.

J.P. Goldblatt and J.C. Richmond. Anatomy and biomechanics of the knee. *Operative Techniques in Sports Medicine*, 11(3):172–186, 2003. ISSN 1060-1872. URL https://doi.org/10.1053/otsm.2003.35911. The Multiple Ligament Injured Knee, Part I.

M.B. Goldring. Articular cartilage degradation in osteoarthritis. *HSS Journal®*, 8(1):7–9, 2012. URL https://doi.org/10.1007/s11420-011-9250-z.

M. Gómez-Florit, R.M.A. Domingues, S.M. Bakht, et al. 1.3.6 – natural materials. In W.R. Wagner, S.E. Sakiyama-Elbert, G. Zhang, et al.,

editors, *Biomaterials Science*, pages 361–375. Academic Press, 4th edition, 2020. ISBN 978-0-12-816137-1. URL https://doi.org/10.1016/B978-0-12-816137-1.00026-X.

E. Hamsayeh Abbasi Niasar and L.P. Li. Characterizing site-specific mechanical properties of knee cartilage with indentation-relaxation maps and machine learning. *Journal of the Mechanical Behavior of Biomedical Materials*, 142:105826, 2023. ISSN 1751-6161. URL https://doi.org/10.1016/j.jmbbm.2023.105826.

T.L. Haut Donahue, M.L. Hull, M.M. Rashid, et al. A finite element model of the human knee joint for the study of tibio-femoral contact. *Journal of Biomechanical Engineering*, 124(3):273–280, 2002. ISSN 0148-0731. doi: 10.1115/1.1470171. URL https://doi.org/10.1115/1.1470171.

G.A. Hawker. Osteoarthritis is a serious disease. *Clinical and Experimental Rheumatology*, 37 Suppl 120(5):3–6, 2019. ISSN 0392-856X. URL http://europepmc.org/abstract/med/31621562.

G.A. Holzapfel. *Nonlinear Solid Mechanics: A Continuum Approach for Engineering*. John Wiley & Sons, Chichester, 2000.

D. Johnson, R. Hashaikeh, and N. Hilal. 1 - basic principles of osmosis and osmotic pressure. In N. Hilal, A.F. Ismail, M. Khayet, et al., editors, *Osmosis Engineering*, pages 1–15. Elsevier, 2021. ISBN 978-0-12-821016-1. URL https://doi.org/10.1016/B978-0-12-821016-1.00011-5.

M. Kazemi, L.P. Li, P. Savard, et al. Creep behavior of the intact and meniscectomy knee joints. *Journal of the Mechanical Behavior of Biomedical Materials*, 4(7):1351–1358, 2011. ISSN 1751-6161. URL https://doi.org/10.1016/j.jmbbm.2011.05.004.

C. Kiani, L. Chen, Y.J. Wu, et al. Structure and function of aggrecan. *Cell Research*, 12(1):19–32, 2002. ISSN 1748-7838. URL https://doi.org/10.1038/sj.cr.7290106.

B. Kim, S.B. Lee, J. Lee, et al. A comparison among neo-Hookean model, Mooney-Rivlin model, and Ogden model for chloroprene rubber. *International Journal of Precision Engineering and Manufacturing*, 13(5):759–764, 2012. ISSN 2005-4602. URL https://doi.org/10.1007/s12541-012-0099-y.

V. Klika, E.A. Gaffney, Y.C. Chen, et al. An overview of multiphase cartilage mechanical modelling and its role in understanding function and pathology. *Journal of the Mechanical Behavior of Biomedical Materials*, 62:139–157, 2016. ISSN 1751-6161. URL https://doi.org/10.1016/j.jmbbm.2016.04.032.

S.M. Klisch. Internally constrained mixtures of elastic continua. *Mathematics and Mechanics of Solids*, 4(4):481–498, 1999. URL https://doi.org/10.1177/108128659900400405.

H. Kong, X.Q. Wang, and X.A. Zhang. Exercise for osteoarthritis: A literature

review of pathology and mechanism. *Frontiers in Aging Neuroscience*, 14, 2022. ISSN 1663-4365. URL https://doi.org/10.3389/fnagi.2022.854026.

J. Korsawe, G. Starke, W. Wang, et al. Finite element analysis of poro-elastic consolidation in porous media: Standard and mixed approaches. *Computer Methods in Applied Mechanics and Engineering*, 195(9):1096–1115, 2006. ISSN 0045-7825. URL https://doi.org/10.1016/j.cma.2005.04.011.

M.J. Lespasio, N.S. Piuzzi, M.E. Husni, et al. Knee osteoarthritis: A primer. *The Permanente Journal*, 21:16–183, 2017. ISSN 1552-5767. URL https://doi.org/10.7812/tpp/16-183.

T. Lin, Y. Wang, X. Liu, et al. A survey of transformers. *AI Open*, 3:111–132, 2022. ISSN 2666-6510. URL https://doi.org/10.1016/j.aiopen.2022.10.001.

W. Lin, Q. Meng, J. Li, et al. The effect of highly inhomogeneous biphasic properties on mechanical behaviour of articular cartilage. *Computer Methods and Programs in Biomedicine*, 206:106122, 2021. ISSN 0169-2607. URL https://doi.org/10.1016/j.cmpb.2021.106122.

R.F. Loeser, J.A. Collins, and B.O. Diekman. Ageing and the pathogenesis of osteoarthritis. *Nature Reviews Rheumatology*, 12(7):412–420, 2016. ISSN 1759-4804. URL https://doi.org/10.1038/nrrheum.2016.65.

R. Lostado Lorza, F. Somovilla Gomez, M. Corral Bobadilla, et al. Comparative analysis of healthy and cam-type femoroacetabular impingement (FAI) human hip joints using the finite element method. *Applied Sciences*, 11(23), 2021. ISSN 2076-3417. URL https://doi.org/10.3390/app112311101.

X.L. Lu and V.C. Mow. Biomechanics of articular cartilage and determination of material properties. *Medicine & Science in Sports & Exercise*, 40(2), 2008. ISSN 0195-9131. URL https://doi.org/10.1249/mss.0b013e31815cb1fc.

E.S. Mameri, S.P. Dasari, L.M. Fortier, et al. Review of meniscus anatomy and biomechanics. *Current Reviews in Musculoskeletal Medicine*, 15 (5):323–335, 2022. ISSN 1935-9748. URL https://doi.org/10.1007/s12178-022-09768-1.

D. Martínez-Moreno, G. Jiménez, P. Gálvez-Martín, et al. Cartilage biomechanics: A key factor for osteoarthritis regenerative medicine. *Biochimica et Biophysica Acta (BBA) - Molecular Basis of Disease*, 1865(6):1067–1075, 2019. ISSN 0925-4439. URL https://doi.org/10.1016/j.bbadis.2019.03.011.

S.A. Mirmojarabian, A.W. Kajabi, J.H.J. Ketola, et al. Machine learning prediction of collagen fiber orientation and proteoglycan content from multiparametric quantitative MRI in articular cartilage. *Journal of Magnetic Resonance Imaging*, 57(4):1056–1068, 2023. URL https://doi.org/10.1002/jmri.28353.

A. Mobasheri, M.P. Rayman, O. Gualillo, et al. The role of metabolism in the pathogenesis of osteoarthritis. *Nature Reviews Rheumatology*, 13(5):302–311, 2017. ISSN 1759-4804. URL https://doi.org/10.1038/nrrheum.2017.50.

M. Motavalli, O. Akkus, and J.M. Mansour. Depth-dependent shear behavior

of bovine articular cartilage: Relationship to structure. *Journal of Anatomy*, 225(5):519–526, 2014. URL https://doi.org/10.1111/joa.12230.

V.C. Mow, S.C. Kuei, W.M. Lai, et al. Biphasic creep and stress relaxation of articular cartilage in compression: Theory and experiments. *Journal of Biomechanical Engineering*, 102(1):73–84, 1980. ISSN 0148-0731. doi: 10.1115/1.3138202. URL https://doi.org/10.1115/1.3138202.

H. Naghibi Beidokhti, D. Janssen, M. Khoshgoftar, et al. A comparison between dynamic implicit and explicit finite element simulations of the native knee joint. *Medical Engineering & Physics*, 38(10):1123–1130, 2016. ISSN 1350-4533. URL https://doi.org/10.1016/j.medengphy.2016.06.001.

V. Nair and G.E. Hinton. Rectified linear units improve restricted Boltzmann machines. In *Proceedings of the 27th International Conference on International Conference on Machine Learning*, ICML'10, page 807–814, 2010. ISBN 9781605589077. URL https://icml.cc/Conferences/2010/papers/432.pdf.

K. Nakahara, Y. Morita, Y. Tomita, et al. Stress evaluation of articular cartilage chondrocyte cell by using multi-scale finite element method and smoothed particle hydrodynamics method. volume Volume 3: Biomedical and Biotechnology Engineering of *ASME International Mechanical Engineering Congress and Exposition*, 2016. URL https://doi.org/10.1115/IMECE2016-66416.

H. Orava, L. Huang, S.P. Ojanen, et al. Changes in subchondral bone structure

and mechanical properties do not substantially affect cartilage mechanical responses – A finite element study. *Journal of the Mechanical Behavior of Biomedical Materials*, 128:105129, 2022. ISSN 1751-6161. URL https://doi.org/10.1016/j.jmbbm.2022.105129.

G.A. Orozco, P. Tanska, A. Gustafsson, et al. Crack propagation in articular cartilage under cyclic loading using cohesive finite element modeling. *Journal of the Mechanical Behavior of Biomedical Materials*, 131: 105227, 2022. ISSN 1751-6161. URL https://doi.org/10.1016/j.jmbbm.2022.105227.

G. Paiva, S. Bhashyam, G. Thiagarajan, et al. A data-driven surrogate model to connect scales between multi-domain biomechanics simulations. In *Annual International Conference of the IEEE Engineering in Medicine and Biology Society*, pages 3077–3080, 2012. URL https://doi.org/10.1109/EMBC.2012.6346614.

A. Paz, G.A. Orozco, P. Tanska, et al. A novel knee joint model in FEBio with inhomogeneous fibril-reinforced biphasic cartilage simulating tissue mechanical responses during gait: Data from the osteoarthritis initiative. *Computer Methods in Biomechanics and Biomedical Engineering*, 0(0):1–15, 2022. URL https://doi.org/10.1080/10255842.2022.2117548.

A.D. Pearle, R.F. Warren, and S.A. Rodeo. Basic science of articular cartilage and osteoarthritis. *Clinics in Sports Medicine*, 24(1):1–12, 2005. ISSN 0278-5919. URL https://doi.org/10.1016/j.csm.2004.08.007.

J.M.P. Quiroga, W. Wilson, K. Ito, et al. Relative contribution of articular cartilage's constitutive components to load support depending on strain rate. *Biomechanics and Modeling in Mechanobiology*, 16(1):151–158, 2017. ISSN 1617-7940. URL https://doi.org/10.1007/s10237-016-0807-0.

P. Riba, A. Fischer, J. Lladós, et al. Learning graph distances with message passing neural networks. In *24th International Conference on Pattern Recognition (ICPR)*, pages 2239–2244, 2018. URL https://doi.org/10.1109/ICPR.2018.8545310.

D.E. Rumelhart, G.E. Hinton, and R.J. Williams. Learning representations by back-propagating errors. *Nature*, 323(6088):533–536, 1986. ISSN 1476-4687. URL https://doi.org/10.1038/323533a0.

S.S. Sajjadinia and M. Haghpanahi. A parametric study on the mechanical role of fibrillar rotations in an articular cartilage finite element model. *Scientia Iranica*, 28(2):830–836, 2021. ISSN 1026-3098. URL https://dx.doi.org/10.24200/sci.2020.51785.2362.

S.S. Sajjadinia, M. Haghpanahi, and M. Razi. Computational simulation of the multiphasic degeneration of the bone-cartilage unit during osteoarthritis via indentation and unconfined compression tests. *Proceedings of the Institution of Mechanical Engineers, Part H: Journal of Engineering in Medicine*, 233(9):871–882, 2019. URL https://doi.org/10.1177/0954411919854011.

S.S. Sajjadinia, B. Carpentieri, and G.A. Holzapfel. A backward pre-stressing algorithm for efficient finite element implementation of in vivo material

and geometrical parameters into fibril-reinforced mixture models of articular cartilage. *Journal of the Mechanical Behavior of Biomedical Materials*, 114:104203, 2021a. ISSN 1751-6161. URL https://doi.org/10.1016/j.jmbbm.2020.104203.

S.S. Sajjadinia, B. Carpentieri, and G.A. Holzapfel. A pointwise evaluation metric to visualize errors in machine learning surrogate models. In A.J. Tallón-Ballesteros, editor, *Proceedings of CECNet 2021*, volume 345 of *Frontiers in Artificial Intelligence and Applications*, pages 26–34. IOS Press, 2021b. URL http://dx.doi.org/10.3233/FAIA210386.

S.S. Sajjadinia, B. Carpentieri, D. Shriram, et al. Multi-fidelity surrogate modeling through hybrid machine learning for biomechanical and finite element analysis of soft tissues. *Computers in Biology and Medicine*, 148:105699, 2022. ISSN 0010-4825. URL https://doi.org/10.1016/j.compbiomed.2022.105699.

T. Salimans and D.P. Kingma. Weight normalization: A simple reparameterization to accelerate training of deep neural networks. In D. Lee, M. Sugiyama, U. Luxburg, et al., editors, *Advances in Neural Information Processing Systems*, volume 29. Curran Associates, Inc., 2016. URL https://proceedings.neurips.cc/paper/2016/file/ed265bc903a5a097f61d3ec064d96d2e-Paper.pdf.

J.H. Salmon, A.C. Rat, J. Sellam, et al. Economic impact of lower-limb osteoarthritis worldwide: A systematic review of cost-of-illness studies. *Os-*

teoarthritis and Cartilage, 24(9):1500–1508, 2016. ISSN 1063-4584. URL https://doi.org/10.1016/j.joca.2016.03.012.

R. Shirazi and A. Shirazi-Adl. Deep vertical collagen fibrils play a significant role in mechanics of articular cartilage. *Journal of Orthopaedic Research*, 26(5):608–615, 2008. URL https://doi.org/10.1002/jor.20537.

A. Sperduti and A. Starita. Supervised neural networks for the classification of structures. *IEEE Transactions on Neural Networks*, 8(3):714–735, 1997. URL https://doi.org/10.1109/72.572108.

M.E. Stender, C.B. Raub, K.A. Yamauchi, et al. Integrating qPLM and biomechanical test data with an anisotropic fiber distribution model and predictions of TGF-β1 and IGF-1 regulation of articular cartilage fiber modulus. *Biomechanics and Modeling in Mechanobiology*, 12(6):1073–1088, 2013. ISSN 1617-7940. URL https://doi.org/10.1007/s10237-012-0463-y.

K. Terzaghi. *Theoretical Soil Mechanics*. Hoboken, NJ, USA: John Wiley & Sons, Inc, 1943.

A. Vulović, G. Filardo, and N. Filipović. Comparison of mechanical response of knee joint with healthy and damaged femoral cartilage. In *IEEE 21st International Conference on Bioinformatics and Bioengineering (BIBE)*, pages 1–4, 2021. URL https://doi.org/10.1109/BIBE52308.2021.9635319.

P.S. Walker and M.J. Erkman. The role of the menisci in force transmission across the knee. *Clinical Orthopaedics and Related Research*,

(109):184–192, 1975. ISSN 0009-921X. URL https://doi.org/10.1097/00003086-197506000-00027.

M. Wang and N. Yang. Three-dimensional computational model simulating the fracture healing process with both biphasic poroelastic finite element analysis and fuzzy logic control. *Scientific Reports*, 8(1):6744, 2018. ISSN 2045-2322. URL https://doi.org/10.1038/s41598-018-25229-7.

X. Wang, T.S.E. Eriksson, T. Ricken, et al. On incorporating osmotic pre-stretch/prestress in image-driven finite element simulations of cartilage. *Journal of the Mechanical Behavior of Biomedical Materials*, 86:409–422, 2018. ISSN 1751-6161. URL https://doi.org/10.1016/j.jmbbm.2018.06.014.

W. Wilson, C.C. van Donkelaar, B. van Rietbergen, et al. Stresses in the local collagen network of articular cartilage: A poroviscoelastic fibril-reinforced finite element study. *Journal of Biomechanics*, 37(3):357–366, 2004. ISSN 0021-9290. URL https://doi.org/10.1016/S0021-9290(03)00267-7.

W. Wilson, C.C. van Donkelaar, B. van Rietbergen, et al. A fibril-reinforced poroviscoelastic swelling model for articular cartilage. *Journal of Biomechanics*, 38(6):1195–1204, 2005. ISSN 0021-9290. URL https://doi.org/10.1016/j.jbiomech.2004.07.003.

W. Wilson, J.M. Huyghe, and C.C. van Donkelaar. Depth-dependent compressive equilibrium properties of articular cartilage explained by its composi-

tion. *Biomechanics and Modeling in Mechanobiology*, 6(1):43–53, 2007. ISSN 1617-7940. URL https://doi.org/10.1007/s10237-006-0044-z.

Z. Wu, S. Pan, F. Chen, et al. A comprehensive survey on graph neural networks. *IEEE Transactions on Neural Networks and Learning Systems*, 32 (1):4–24, 2021. URL https://doi.org/10.1109/tnnls.2020.2978386.

J. Xu, X. Sun, Z. Zhang, et al. Understanding and improving layer normalization. In H. Wallach, H. Larochelle, A. Beygelzimer, et al., editors, *Advances in Neural Information Processing Systems*, volume 32. Curran Associates, Inc., 2019. URL https://proceedings.neurips.cc/paper/2019/file/2f4fe03d77724a7217006e5d16728874-Paper.pdf.

Y. Yang and P. Perdikaris. Conditional deep surrogate models for stochastic, high-dimensional, and multi-fidelity systems. *Computational Mechanics*, 64(2):417–434, 2019. ISSN 1432-0924. URL https://doi.org/10.1007/s00466-019-01718-y.

Y. Yu, X. Si, C. Hu, et al. A review of recurrent neural networks: LSTM cells and network architectures. *Neural Computation*, 31(7):1235–1270, 2019. ISSN 0899-7667. URL https://doi.org/10.1162/neco_a_01199.

L. Zhang, Y. Wu, P. Jiang, et al. A multi-fidelity surrogate modeling approach for incorporating multiple non-hierarchical low-fidelity data. *Advanced Engineering Informatics*, 51:101430, 2022. ISSN 1474-0346. URL https://doi.org/10.1016/j.aei.2021.101430.

J. Zhou, G. Cui, S. Hu, et al. Graph neural networks: A review of methods

and applications. *AI Open*, 1:57–81, 2020. ISSN 2666-6510. URL https://doi.org/10.1016/j.aiopen.2021.01.001.

Biographies

Seyed Shayan Sajjadinia is currently a PhD student in computer science at the Faculty of Engineering, University of Bozen-Bolzano with also an educational background in biomechanical engineering. His research interest is application of deep learning and finite element analysis in computer simulation, especially in advanced biomechanical analysis, which is the focus of his PhD research dissertation.

Bruno Carpentieri earned a Laurea degree in applied mathematics from Bari University in 1997 and then pursued his PhD studies in computer science at Toulouse, France. He has gained professional experience as a postdoctoral researcher at the University of Graz, as an Assistant Professor at the University of Groningen, and as a Reader at Nottingham Trent University. Since May 2017, he holds the position of Associate Professor in Applied Mathematics at the Faculty of Engineering, University of Bozen-Bolzano. His research expertise is numerical linear algebra and high-performance computing.

Gerhard A. Holzapfel is a Professor and head of the Institute of Biomechanics at Graz University of Technology, an Adjunct Professor at the Norwegian University of Science and Technology and a Visiting Professor at the University of Glasgow. He has made significant contributions in the field of experimental and computational biomechanics, with a particular interest in soft biological tissues. He has received numerous awards and honors for his work and

is listed in ‘The World’s Most Influential Scientific Minds: 2014’ by Thomas Reuters. Professor Holzapfel is also the co-founder and co-editor-in-chief of the journal of Biomechanics and Modeling in Mechanobiology.